Nuclear level density and γ-ray strength function of ^{63}Ni

V. W. Ingeberg [1] P. Jones [2] L. Msebi,[2,3] S. Siem,[1] M. Wiedeking [2,4] A. A. Avaa,[2,4] M. V. Chisapi,[2,5]
E. A. Lawrie [2,3] K. L. Malatji [2,5] L. Makhathini,[2] S. P. Noncolela,[2,3] and O. Shirinda [6]

[1]*Department of Physics, University of Oslo, N-0316 Oslo, Norway*
[2]*SSC Laboratory, iThemba LABS, P.O. Box 722, 7129 Somerset West, South Africa*
[3]*Physics Department, University of the Western Cape, P/B X17, Bellville 7535, South Africa*
[4]*School of Physics, University of the Witwatersrand, 2050 Johannesburg, South Africa*
[5]*Physics Department, Stellenbosch University, P/B X1, Matieland 7602, South Africa*
[6]*Department of Physical and Earth Sciences, Sol Plaatje University, Private Bag X5008, Kimberley 8301, South Africa*

The nuclear level density (NLD) and γ-ray strength function (γSF) of ^{63}Ni have been investigated using the Oslo method. The extracted NLD is compared with previous measurements using particle evaporation and those found from neutron resonance spacing. The γSF was found to feature a strong low-energy enhancement that could be explained as $M1$ strength based on large-scale shell model calculations. Comparison of γSFs measured with the Oslo method for various Ni isotopes reveals systematic changes to the strength below 5 MeV with increasing mass.

I. INTRODUCTION

Statistical properties of nuclei such as the nuclear level density (NLD) and γ-ray strength function (γSF) provide valuable insight into the structure of the nucleus. Such nuclear data are also vital for many applications [1,2], for example astrophysics [3], advanced fuel cycles [4], and nuclear waste transmutation [5]. Measurements of NLDs and γSFs are particularly important for those applications when reaction cross sections cannot be measured through direct techniques, since they are essential input for statistical reaction theory [6].

The Oslo method is a powerful analytical method that allows for simultaneous extraction of nuclear level density and γ-ray strength functions from particle-γ coincidences following reactions with light ion beams [e.g., (p, p'), (d, p) etc.] [7]. The method has been extended to be used in conjunction with total absorption spectrometry following β decay (β-Oslo method) [8], and particle-γ coincidences from inverse-kinematics experiments [9].

The Oslo method itself does not provide the absolute NLD and γSF values, but rather the functional shapes. In order to determine the correct common slope of the NLD and γSF, as well as their absolute values, a normalization to auxiliary experimental data is required. Typical data for normalization are the s-wave resonance spacing, discrete resolved levels, and average radiative width. The reliance on external data means that the accuracy of the final NLD and γSF is mostly determined by the accuracy of those data. The resonance spacings and radiative widths can be highly uncertain, especially in nuclei with few resonances. For the majority of unstable nuclei these have not even been measured. This means

that alternative approaches for normalization have to be used especially for cases where no experimental resonance data are available. For nuclei close to stability these values can typically be estimated from systematics in the vicinity of the nucleus using models [8]. The downside of such normalized NLDs and γSFs is the introduction of model dependencies, which may result in large uncertainties. A model-independent approach is the use of the Shape method [10,11] to determine the slope of the γSF, however, the method requires sufficient particle energy resolution and a well-known level structure with resolvable energy spacing at low excitation energy. In this paper we will look at a possible third option in which only NLD from known discrete states is used to normalize the NLD. Provided the discrete level scheme is sufficiently complete, such an approach will result in a model-independent normalization of the NLD. This may be particularly important for measurements in nuclei far away from stability where NLD models have not been assessed.

In this paper we have analyzed data from a (p, d) reaction on ^{64}Ni to measure the NLD and γSF of ^{63}Ni. The level density of ^{63}Ni has previously been measured using particle evaporation spectra and shows significantly lower NLD than that expected from resonance spacing data [12,13]. This makes ^{63}Ni a very interesting case study as a normalization only considering known discrete levels could resolve the discrepancy. In addition, the γSFs have previously been measured in several other Ni isotopes and consistently show a strong low-energy enhancement [14–19]. With this measurement the NLD and γSF will have been measured in most stable [14–16,20] and several unstable Ni isotopes [17–20], allowing for investigations into the systematics of the γSF.
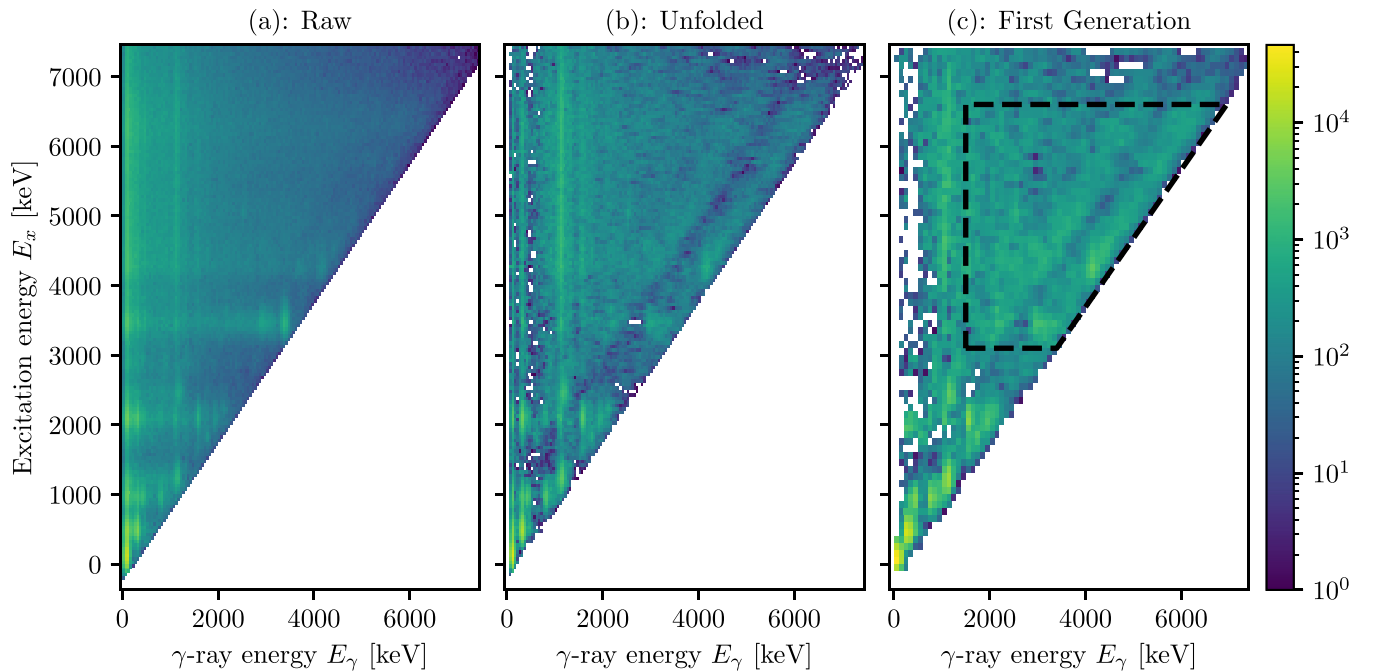
FIG. 1. The (a) raw, (b) unfolded, and (c) first generation matrix. See text for details.

II. EXPERIMENT AND ANALYSIS

The experiment measuring particle-γ coincidences from the ^{64}Ni(p, d)^{63}Ni reaction was performed with a 27.4 MeV proton beam accelerated by the Separated Sector Cyclotron (SSC) at iThemba LABS. The 4.56 mg/cm^2 thick ^{64}Ni target was bombarded with a beam current of $\approx$1 pnA for about 15 h at the center of the AFRODITE array [21]. The array consisted of eight Compton suppressed high-purity germanium (HPGe) CLOVER detectors, six small (2 in $\times$ 2 in) and two large volume (3.5 in $\times$ 8 in) LaBr$_3$:Ce detectors. Particles from the reaction were measured by two silicon detectors of the S2 type in a ΔE-E configuration and placed downstream of the target. The ΔE detector had a thickness of 309 μm and the E detector was 1041 μm thick. In front of the particle telescope a 10 μm thick aluminum absorber was placed to shield from δ electrons. Signals from the detectors were read out using Pixie-16 digital pulse processors from XIA. Each detector was self-triggering and the pulse height, time stamp, and constant fraction corrections of each event were stored to disk for off-line analysis.

Particle-γ coincidences were found in the list mode data by placing time gates on the prompt time peak in the particle-γ time spectra. Background events were found by placing an off-prompt time gate of similar length. The mass and charge of the ejected particle, and thus the reaction channel, was selected by applying a graphical cut in the ΔE vs. E matrix. For each event the excitation energy of the residual ^{63}Ni nucleus was found from kinematic reconstruction assuming a two-body reaction. The resulting excitation energy and coincident γ-ray spectrum were then used to construct the prompt excitation versus γ-ray energy matrix shown in Fig. 1(a). A similar background excitation-γ-ray energy matrix was constructed from the events in the background time gate.

After applying time and particle gates a total of 3.7×10^6, 4.8×10^6, and 5.7×10^6 prompt particle-γ coincidences and 7.3×10^5, 1.0×10^6, and 7.9×10^5 background events were found in the CLOVER, large LaBr$_3$:Ce and small LaBr$_3$:Ce detectors, respectively. The considerably lower background to prompt ratio for the small LaBr$_3$:Ce detectors can be attributed to their exceptionally high time resolution [22]. In the following analysis only particle-γ coincidences in the large LaBr$_3$:Ce detectors were considered as these exhibit far superior efficiency at high γ-ray energies, which is important in the Oslo method.

A. Oslo method

The starting point for the Oslo method is the excitation-γ matrix. The first step is to correct for the response of the γ detector using the unfolding method [23]. The response function of the setup was found from simulations of the AFRODITE array using a model implemented in GEANT4 [24,25]. The resulting unfolded matrix is shown in Fig. 1(b). The peak at $E_x = 3.6$ MeV to the ground state was fitted and subtracted from the unfolded spectra with the justification being that this state is only populated directly from the reaction and has no feeding from the quasicontinuum.

Next is to find the first generation matrix using the first generation method [26]. The resulting first generation matrix contains the distribution of the first γ rays emitted in cascades depopulating each excitation bin and is shown in Fig. 1(c).

The first generation matrix is proportional to the NLD and γ-ray transmission coefficient via [7]

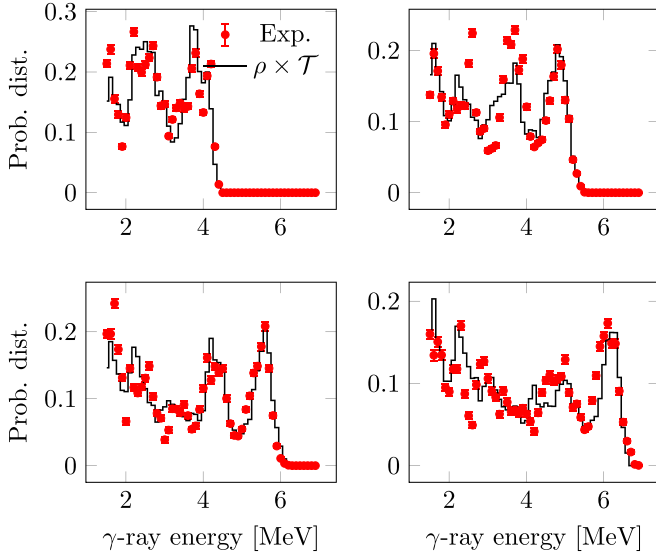$$\Gamma(E_\gamma, E_x) \propto \mathcal{T}(E_\gamma)\rho(E_x - E_\gamma), \tag{1}$$

FIG. 2. ^{63}Ni primary γ-ray distribution at excitation energy 4 MeV (top left), 5 MeV (top right), 5.75 MeV (bottom left), and 6.4 MeV (bottom right). Red dots show the experimental first generation spectra, while the solid black line is the product of the fitted NLD and γSF.

where $\Gamma(E_\gamma, E_x)$ is the bin with γ-ray energy E_γ and excitation energy E_x. $\mathcal{T}(E_\gamma)$ is the transmission coefficient for γ-ray energy E_γ and $\rho(E_x - E_\gamma)$ is the level density at the final excitation energy $E_f = E_x - E_\gamma$. The NLD and γ-ray transmission coefficients are extracted from the first generation matrix by fitting a theoretical matrix

$$\Gamma_{\text{th}}(E_\gamma, E_x) = \frac{\rho(E_x - E_\gamma)\mathcal{T}(E_\gamma)}{\sum\limits_{E_\gamma = E_\gamma^{\min}}^{E_x} \rho(E_x - E_\gamma)\mathcal{T}(E_\gamma)}, \quad (2)$$

where $\rho(E_x - E_\gamma)$ and $\mathcal{T}(E_\gamma)$ are treated as free variables for each final energy $E_f = E_x - E_\gamma$ and γ-ray energy E_γ. The fit was done by minimizing

$$\chi^2 = \sum_{E_x, E_\gamma} \left(\frac{\Gamma(E_\gamma, E_x) - \Gamma_{\text{th}}(E_\gamma, E_x)}{\Delta \Gamma(E_\gamma, E_x)} \right)^2. \quad (3)$$

The region of the first generation matrix fitted was limited to a minimum γ-ray energy of 1500 keV and excitation energies between 3100 keV and 6600 keV to ensure only statistical decay was included. The region is highlighted by the dashed line in Fig. 1(c). The resulting theoretical first generation matrix are shown for a few select excitation bins together with the experimental matrix in Fig. 2.

The NLD and γ-ray transmission coefficients resulting from the χ^2 minimization are not the physical values, but rather the shape as Eq. (3) is symmetric under transformation

$$\tilde{\rho}(E_x - E_\gamma) = A\rho(E_x - E_\gamma)e^{\alpha(E_x - E_\gamma)}$$

$$\tilde{\mathcal{T}}(E_\gamma) = B\mathcal{T}(E_\gamma)e^{\alpha E_\gamma}, \quad (4)$$

where A, B, and α are transformation parameters. To obtain the physical transformation for the extracted NLD and

γ-transmission coefficients, a normalization to external data has to be performed, see Sec. III. The γSF is related to the transmission coefficient via $f(E_\gamma) = \mathcal{T}(E_\gamma)/(2\pi E_\gamma^3)$, under the assumption that dipole transitions dominate the transmission coefficients.

III. NORMALIZATION OF LEVEL DENSITY AND γ-RAY STRENGTH FUNCTION

The main auxiliary data required to normalize the NLD is known level densities from tabulated levels and the NLD at the neutron separation energy S_n. Tabulated levels are converted to level density simply by counting the number of levels within each excitation bin and dividing by the bin width. This results in a level density that will have large fluctuations compared to Oslo method data as the experimental resolution has not yet been accounted for. The level density from known levels is smoothed with a Gaussian with FWHM of about 325 keV to match the experimental resolution for final excitation energy. Tabulated discrete levels were taken from the RIPL-3 library [27].

The level density at the neutron separation energy is found from the resonance spacing of s-wave resonances D_0 by [7]

$$\rho(S_n) = \frac{2}{g(S_n, J_t - 1/2) + g(S_n, J_t + 1/2)} \frac{1}{D_0}, \quad (5)$$

where J_t is the ground-state spin of the $A - 1$ nucleus. The spin distribution $g(E_x, J)$ is given by the Ericson distribution [28]

$$g(E_x, J) = \exp\left(-\frac{J^2}{2\sigma^2(E_x)}\right) - \exp\left(-\frac{(J+1)^2}{2\sigma^2(E_x)}\right), \quad (6)$$

with the spin-cutoff parameter parameterized by [29]

$$\sigma^2(E_x) = \begin{cases} \sigma_d^2 & E < E_d \\ \sigma_d^2 + \frac{E - E_d}{S_n - E_d}\left(\sigma^2(S_n) - \sigma_d^2\right) & E \geqslant E_d. \end{cases} \quad (7)$$

The spin-cutoff parameter of the discrete levels ($E_d = 2.0$ MeV) is estimated to be $\sigma_d = 2.30(23)$ from tabulated discrete levels [27] and large-scale shell model calculations [30], while the spin-cutoff parameter at the neutron separation energy was estimated to be $\sigma(S_n) = 3.68(21)$ estimated from the models of Refs. [31–33]. The s-wave resonance spacing $D_0 = 16.0(30)$ keV was taken from Refs. [27,34,35] resulting in a total level density at the neutron separation energy of $1730(363)$ MeV^{-1}.

The experimental NLD only extends up to 5.2 MeV and to properly compare with the level density at the neutron separation energy the NLD is extrapolated to S_n via a constant temperature (CT) formula [28]

$$\rho_{\text{CT}}(E_x) = \frac{1}{T} \exp\left(\frac{E_x - E_{\text{shift}}}{T}\right), \quad (8)$$

where the temperature T and shift parameter E_{shift} are treated as free parameters.

Data required to normalize the γSF is the average radiative width of s-wave resonances, as this value is related to the γSF

TABLE I. List of parameters used to normalize the NLD and γSF. The spin-cutoff at S_n $\sigma(S_n)$ is estimated from the model predictions of [31–33] while the discrete levels spin-cutoff is estimated from the discrete states [27] and shell model calculations [30]. The s-wave resonance spacing D_0 are taken from Refs. [27,34,35], while the $\langle\Gamma_\gamma\rangle$ is a weighted average of tabulated radiative widths in Ref. [34].

S_n	6.838 MeV
D_0	16.0(30) keV
$\sigma(S_n)$	3.63(21)
E_d	2.0 MeV
$\sigma(E_d)$	2.3(23)
$\langle\Gamma_\gamma\rangle$	534(214) MeV
$\rho(S_n)$	1730(363) 1/MeV

and NLD via [36]

$$\langle\Gamma_{\gamma 0}\rangle = \frac{D_0}{2}\int_0^{S_n} dE_\gamma E_\gamma^3 f(E_\gamma)\rho(S_n - E_\gamma)$$
$$\times [g(S_n - E_\gamma, 1/2) + g(S_n - E_\gamma, 3/2)]E_\gamma. \quad (9)$$

Due to the limits selected (see Sec. II A) for the extraction of the NLD and γSF the experimental data only extends up to $E_x = 5.2$ MeV and E_γ between 1.5 and 6.6 MeV, respectively. To evaluate the integral in Eq. (9) the NLD was extrapolated with the constant temperature formula, Eq. (8), between 5.2 MeV and the neutron separation energy. The γSF was extrapolated using $f(E_\gamma) = Ce^{\eta E_\gamma}$, and $f(E_\gamma) = Ce^{\eta E_\gamma}/E_\gamma^3$ for energies between 0 and 1.5 MeV, and 6.6 MeV and the neutron separation energy, respectively. The average radiative width of s-wave resonances in ^{63}Ni was found to be 534(214) MeV by a weighted average of all the tabulated values found in Ref. [34]. Due to the large spread of the tabulated values a large uncertainty of 40% was assumed. All normalization parameters adopted in this analysis are listed in Table I. The normalization parameters A, B, and α were found by sampling the posterior probability distribution with total likelihood function

$$\mathcal{L}(\boldsymbol{\theta}) = \prod_i \mathcal{L}_i(\boldsymbol{\theta}), \quad (10)$$

using the Bayesian sampling package ULTRANEST [37]. All experimental data are assumed to be normally distributed, giving the likelihoods

$$\ln\mathcal{L}_{\text{discrete}} = \sum_i \ln\frac{1}{\sqrt{2\pi}\sigma_{j,\text{Oslo}}(\boldsymbol{\theta})}$$
$$- \frac{1}{2}\sum_i \left(\frac{\rho_{j,\text{discrete}} - \rho_{j,\text{Oslo}}(\boldsymbol{\theta})}{\sigma_{j,\text{Oslo}}(\boldsymbol{\theta})}\right)^2, \quad (11)$$

$$\ln\mathcal{L}_{\text{CT}} = \sum_i \ln\frac{1}{\sqrt{2\pi}\sigma_{j,\text{Oslo}}(\boldsymbol{\theta})}$$
$$- \frac{1}{2}\sum_i \left(\frac{\rho_{j,\text{CT}} - \rho_{j,\text{Oslo}}(\boldsymbol{\theta})}{\sigma_{j,\text{Oslo}}(\boldsymbol{\theta})}\right)^2, \quad (12)$$
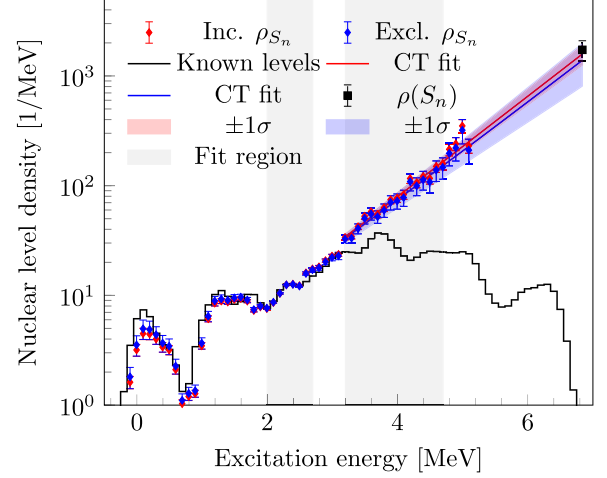

FIG. 3. The extracted and normalized NLD. The red and blue circles are the experimental values, while the black solid line is the level density from the known resolved levels convoluted with the experimental resolution. The black solid square is the level density at the neutron separation energy found from the s-wave resonance spacing reported by [27,34,35]. The red solid line shows the level density from the fitted CT model while the red shaded area is the $\pm 1\sigma$ confidence interval.

$$\ln\mathcal{L}_{\rho_{S_n}} = \left(\frac{\rho_{S_n} - \rho_{S_n,\text{CT}}(\boldsymbol{\theta})}{\sigma_{\rho_{S_n}}}\right)^2, \quad (13)$$

$$\ln\mathcal{L}_{\langle\Gamma_{\gamma 0}\rangle} = \left(\frac{\langle\Gamma_{\gamma 0}\rangle_{\text{exp}} - \langle\Gamma_{\gamma 0}\rangle_{\text{Oslo}}(\boldsymbol{\theta})}{\sigma_{\langle\Gamma_{\gamma 0}\rangle_{\text{exp}}}}\right)^2. \quad (14)$$

The parameters $\boldsymbol{\theta} = (A, B, \alpha, T, E_{\text{shift}}, \sigma_D, \sigma_{S_n})$ have a uniform prior between 0 and 5 for A and B and -1 MeV^{-1} and 1 MeV^{-1} for α. The temperature and shift parameters also used a uniform prior between 0.2 and 2 MeV and -10 and 10 MeV, respectively. The spin-cutoff parameters were included as nuance parameters with normal distributed priors to ensure proper propagation of errors. The resulting normalized NLD and γSF are shown as red circles in Figs. 3 and 4, respectively. The discrete likelihood, Eq. (11) was limited to data points between 2 and 2.7 MeV, while the CT formula was fitted between 3.2 and 4.7 MeV. To investigate the sensitivity to the resonance spacing the analysis was repeated, but excluding Eq. (13) in the total likelihood and resulted in the NLD and γSF shown as blue circles in Figs. 3 and 4, respectively.

In many cases, normalization of the NLD and γSF can be further constrained by applying the Shape method [10,11], such as in the cases of $^{142,144-151}$Nd [38] and ^{120}Sn [39]. Here however, we did not pursue this option as poor excitation energy resolution prevented us from distinguishing between decays to levels with known and unknown spins and parities.

IV. DISCUSSION AND COMPARISON

A. Level density

We find that the experimental NLD fits exceptionally well with the tabulated discrete NLD up to about $E_x \approx 3.6$ MeV
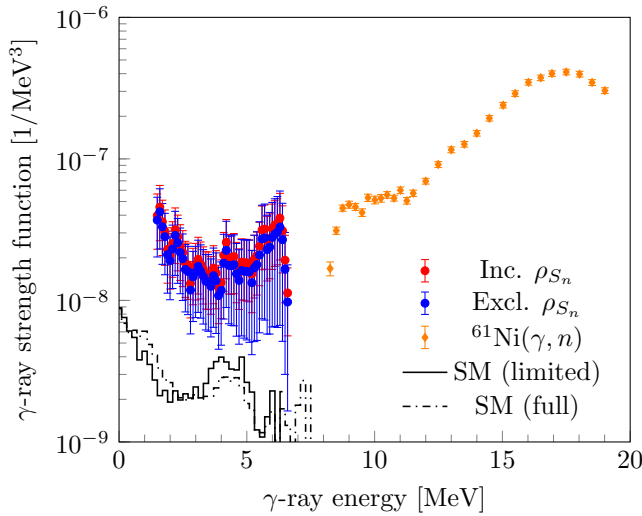
FIG. 4. Extracted γSF when including the NLD at S_n from resonance spacings in the normalization are shown by the red circles while the blue circles only consider the level density from known levels. The orange diamonds are the γSF of ^{61}Ni measured by Ref. [16]. The black line shows the calculated $M1$ strength from shell model calculations [30] considering only decay from levels within the fit region, while the dash-dotted line includes all levels found in the shell model calculation.

indicating that the level scheme might be complete up to even higher excitation energies, than the evaluated $E_x = 2.7$ MeV [27].

Comparing the two normalizations we see that the one including $\rho(S_n)$ results in a slightly steeper slope. Overall the two normalizations are well within the error bars of each other demonstrating that normalizations without knowledge of the NLD at the neutron separation energy are viable.

Figure 5 shows the NLD compared with the experimental NLD found from particle evaporation spectra [12] and the NLD found in large scale shell model (SM) calculations [30]. The SM results clearly overestimate the NLD between 1.8 and 3.7 MeV while underestimating above 4 MeV up to around 6 MeV where the model space seems to be exhausted. The NLD found from evaporation studies fits well within the error bars up to about 4.5 MeV where the presented NLD seems to tend to higher densities.

In Fig. 6 the NLDs of ^{59,60,64,65,67,69,70}Ni [14,15,17–20] are shown together with the measured ^{63}Ni isotope. We observe a trend for $E_x > 2$ MeV with the absolute NLD increasing with mass number. All the odd-A nuclei clearly have higher NLDs, as expected due to the unpaired neutron [40].

B. γ-ray strength function

The extracted γSF features a strong up-bend at low energies similar to what has been seen in other Ni isotopes [14–18,20], as well as other nuclei in the same mass region [41–43]. Comparing the measured strength function to the $M1$ strength predicted from the SM calculations in Ref. [30] we see that qualitatively these have a similar shape, although the absolute values of the SM calculations are con-
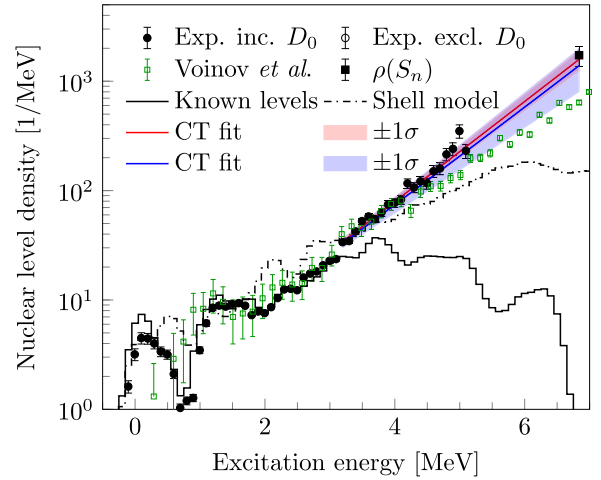

FIG. 5. Comparison between the presented NLD shown by the open and filled black circles and the NLD found in large-scale shell model calculations [30] shown by the dash-dotted line. The black solid square is the level density at the neutron separation energy found from the s-wave resonance spacing reported by Refs. [27,34,35], while the green open boxes represent the NLD found in particle evaporation studies by Voinov et al. [12].

siderably lower. Comparison with the photoabsorption cross section of ^{61}Ni [16] shows a reasonably good agreement as the giant dipole resonance evolves slowly with mass number. The normalized γSF has a considerably large uncertainty band with the dominating contributing factor being the uncertainty in the average radiative width. Excluding the $\rho(S_n)$ in the normalization does also have a large impact on the uncertainties of the normalization for the γSF, increasing the size of the error bars from $\approx 45\%$ to $\approx 80\%$, especially at higher γ-ray energies.

In Fig. 7 we show the γSF for ^{59,60,64,65,67,69,70}Ni [14–19] together with the presented γSF. From this comparison we can see a clear trend with the strength below ≈ 4.5 MeV significantly decreasing with higher mass numbers. This is especially apparent in the unstable neutron-rich nuclei ($A =$
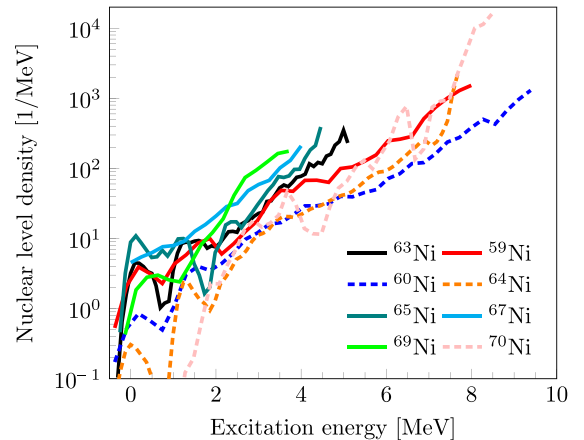

FIG. 6. NLDs measured with the Oslo method in Ni isotopes. The NLDs of ^{59,60,64,65,67,69,70}Ni are taken from Refs. [14,15,17–20].
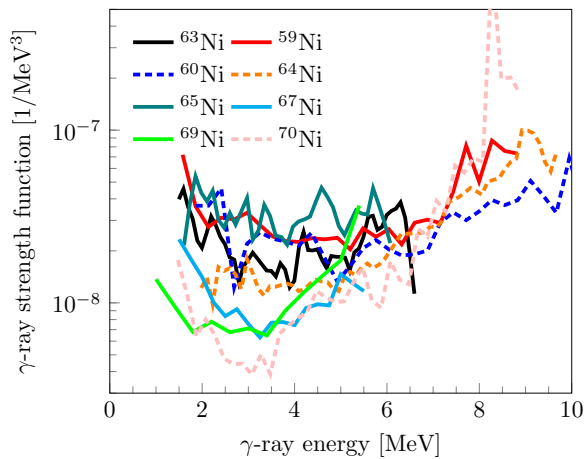
FIG. 7. γSFs measured with the Oslo method in Ni isotopes. The γSFs of ^{59,60,64,65,67,69,70}Ni are taken from Refs. [14–19].

67, 69, and 70). The outlier is the γSF of ^{65}Ni, which have the highest strength overall.

V. SUMMARY

We have measured the NLD and γSF of ^{63}Ni and found that the NLD agrees well with that found from known levels, and are compatible with the NLD at the neutron separation energy found in neutron resonance studies. The NLD of Ref. [12] agrees with the presented NLD for excitation energies up to about 4.7 MeV where the presented NLD seems to be somewhat steeper. Based on this we conclude that our results tend to favor the NLD found in resonance studies, rather than those of Ref. [12]. The reason for the discrepancy remains unknown and warrants further investigation.

The measured γSF features a strong low-energy enhancement similar to that found in other Ni isotopes. Shell model calculations from Ref. [30] suggest that the enhancement may be due to $M1$ transitions within the quasicontinuum. Compared with (γ, n) [16] data for ^{61}Ni there may be a pygmy resonance around 7–8 MeV, but due to the large uncertainties in the absolute value of the measured γSF we cannot conclude.

In general the exclusion of s-wave spacing in the overall fit of the NLD and γSF resulted in very similar results, although with considerably larger uncertainties when extrapolating towards the neutron separation energy. Based on this we can conclude that if the level scheme is sufficiently well known a reasonably good normalization for the NLD can be obtained even without resonance data.

[1] L. A. Bernstein, D. A. Brown, A. J. Koning, B. T. Rearden, C. E. Romano, A. A. Sonzogni, A. S. Voyles, and W. Younes, Our future nuclear data needs, Annu. Rev. Nucl. Part. Sci. **69**, 109 (2019).

[2] S. Goriely, P. Dimitriou, M. Wiedeking, T. Belgya, R. Firestone, J. Kopecky, M. Krtička, V. Plujko, R. Schwengner, S. Siem, H. Utsunomiya, S. Hilaire, S. Péru, Y. S. Cho, D. M. Filipescu, N. Iwamoto, T. Kawano, V. Varlamov, and R. Xu, Reference database for photon strength functions, Eur. Phys. J. A **55**, 172 (2019).

[3] M. Arnould and S. Goriely, Astronuclear physics: A tale of the atomic nuclei in the skies, Prog. Part. Nucl. Phys. **112**, 103766 (2020).

[4] M. B. Chadwick, M. Herman, P. Obložinský, M. E. Dunn, Y. Danon, A. C. Kahler, D. L. Smith, B. Pritychenko, G. Arbanas, R. Arcilla, R. Brewer, D. A. Brown, R. Capote, A. D. Carlson, Y. S. Cho, H. Derrien, K. Guber, G. M. Hale, S. Hoblit, S. Holloway *et al.*, Endf/b-vii.1 nuclear data for science and technology: Cross sections, covariances, fission product yields and decay data, Nucl. Data Sheets **112**, 2887 (2011).

[5] M. Salvatores and G. Palmiotti, Radioactive waste partitioning and transmutation within advanced fuel cycles: Achievements and challenges, Prog. Part. Nucl. Phys. **66**, 144 (2011).

[6] W. Hauser and H. Feshbach, The inelastic scattering of neutrons, Phys. Rev. **87**, 366 (1952).

[7] A. Schiller, L. Bergholt, M. Guttormsen, E. Melby, J. Rekstad, and S. Siem, Extraction of level density and γ strength function from primary γ spectra, Nucl. Instrum. Meth. Phys. Res. A **447**, 498 (2000).

[8] A. Spyrou, S. N. Liddick, A. C. Larsen, M. Guttormsen, K. Cooper, A. C. Dombos, D. J. Morrissey, F. Naqvi, G. Perdikakis, S. J. Quinn, T. Renstrøm, J. A. Rodriguez, A. Simon, C. S. Sumithrarachchi, and R. G. T. Zegers, Novel Technique for Constraining r -Process (n, γ) Reaction Rates, Phys. Rev. Lett. **113**, 232502 (2014).

[9] V. W. Ingeberg, S. Siem, M. Wiedeking, K. Sieja, D. L. Bleuel, C. P. Brits, T. D. Bucher, T. S. Dinoko, J. L. Easton, A. Görgen, M. Guttormsen, P. Jones, B. V. Kheswa, N. A. Khumalo, A. C. Larsen, E. A. Lawrie, J. J. Lawrie, S. N. Majola, K. L. Malatji, L. Makhathini *et al.*, First application of the Oslo method in inverse kinematics, Eur. Phys. J. A **56**, 68 (2020).

[10] M. Wiedeking, M. Guttormsen, A. C. Larsen, F. Zeiser, A. Görgen, S. N. Liddick, D. Mücher, S. Siem, and A. Spyrou, Independent normalization for γ -ray strength functions: The shape method, Phys. Rev. C **104**, 014311 (2021).

[11] D. Mücher, A. Spyrou, M. Wiedeking, M. Guttormsen, A. C. Larsen, F. Zeiser, C. Harris, A. L. Richard, M. K. Smith, A. Görgen, S. N. Liddick, S. Siem, H. Berg, J. A. Clark, P. A. DeYoung, A. C. Dombos, B. Greaves, L. Hicks, R. Kelmar, S. Lyons *et al.*, A novel approach for extracting model-independent nuclear level densities far from stability, arXiv:2011.01071.

[12] A. V. Voinov, S. M. Grimes, C. R. Brune, T. Massey, and A. Schiller, Recent experimental results on level densities for compound reaction calculations, EPJ Web Conf. **21**, 05001 (2012).

[13] B. M. Oginni, S. M. Grimes, A. V. Voinov, A. S. Adekola, C. R. Brune, D. E. Carter, Z. Heinen, D. Jacobs, T. N. Massey, J. E. O'Donnell, and A. Schiller, Test of level density models from reactions of Li6 on Fe58 and Li7 on Fe57, Phys. Rev. C **80**, 034305 (2009).

[14] L. Crespo Campo, F. L. Bello Garrote, T. K. Eriksen, A. Görgen, M. Guttormsen, K. Hadynska-Klek, M. Klintefjord, A. C. Larsen, T. Renstrøm, E. Sahin, S. Siem, A. Springer, T. G. Tornyi, and G. M. Tveten, Statistical γ-decay properties of Ni 64 and deduced (n,γ) cross section of the s-process branch-point nucleus Ni 63, Phys. Rev. C **94**, 044321 (2016).

[15] L. Crespo Campo, A. C. Larsen, F. L. Bello Garrote, T. K. Eriksen, F. Giacoppo, A. Görgen, M. Guttormsen, M. Klintefjord, T. Renstrøm, E. Sahin, S. Siem, T. G. Tornyi, and G. M. Tveten, Investigating the γ decay of Ni 65 from particle-γ coincidence data, Phys. Rev. C **96**, 014312 (2017).

[16] H. Utsunomiya, T. Renstrøm, G. M. Tveten, S. Goriely, S. Katayama, T. Ari-izumi, D. Takenaka, D. Symochko, B. V. Kheswa, V. W. Ingeberg, T. Glodariu, Y. W. Lui, S. Miyamoto, A. C. Larsen, J. E. Midtbø, A. Görgen, S. Siem, L. C. Campo, M. Guttormsen, S. Hilaire *et al.*, Photoneutron cross sections for Ni isotopes: Toward understanding (n,γ) cross sections relevant to weak s-process nucleosynthesis, Phys. Rev. C **98**, 054619 (2018).

[17] A. C. Larsen, J. E. Midtbø, M. Guttormsen, T. Renstrøm, S. N. Liddick, A. Spyrou, S. Karampagia, B. A. Brown, O. Achakovskiy, S. Kamerdzhiev, D. L. Bleuel, A. Couture, L. C. Campo, B. P. Crider, A. C. Dombos, R. Lewis, S. Mosby, F. Naqvi, G. Perdikakis, C. J. Prokop *et al.*, Enhanced low-energy γ-decay strength of Ni 70 and its robustness within the shell model, Phys. Rev. C **97**, 054329 (2018).

[18] A. Spyrou, A. C. Larsen, S. N. Liddick, F. Naqvi, B. P. Crider, A. C. Dombos, M. Guttormsen, D. L. Bleuel, A. Couture, L. C. Campo, R. Lewis, S. Mosby, M. R. Mumpower, G. Perdikakis, C. J. Prokop, S. J. Quinn, T. Renstrom, S. Siem, and R. Surman, Neutron-capture rates for explosive nucleosynthesis: The case of 68Ni(n, γ)69Ni, J. Phys. G: Nucl. Part. Phys. **44**, 044002 (2017).

[19] V. W. Ingeberg, S. Siem, M. Wiedeking, S. Goriely, K. Abrahams, K. Arnswald, F. Bello Garrote, T. Berry, D. L. Bleuel, J. Cederkäll, T. Christoffersen, D. Cox, L. Crespo Campo, H. De Witte, L. Gaffney, A. Görgen, C. Henrich, A. Illana Sison, P. Jones, B. Kheswa *et al.* (unpublished).

[20] T. Renstrøm, G. M. Tveten, J. E. Midtbø, H. Utsunomiya, O. Achakovskiy, S. Kamerdzhiev, B. A. Brown, A. Avdeenkov, T. Ari-izumi, A. Görgen, S. M. Grimes, M. Guttormsen, T. W. Hagen, V. W. Ingeberg, S. Katayama, B. V. Kheswa, A. C. Larsen, Y. W. Lui, H. T. Nyhus, S. Siem *et al.*, Experimental γ-decay strength in ^{59,60}Ni compared with microscopic calculations, arXiv:1804.08086.

[21] M. Lipoglavšek, A. Likar, M. Vencelj, T. Vidmar, R. A. Bark, E. Gueorguieva, F. Komati, J. J. Lawrie, S. M. Maliage, S. M. Mullins, S. H. Murray, and T. M. Ramashidzha, Measuring high-energy γ-rays with Ge clover detectors, Nucl. Instrum. Meth. Phys. Res. A **557**, 523 (2006).

[22] L. Msebi, V. W. Ingeberg, P. Jones, J. F. Sharpey-Schafer, A. A. Avaa, T. D. Bucher, C. P. Brits, M. V. Chisapi, D. J. C. Kenfack, E. A. Lawrie, K. L. Malatji, B. Maqabuka, L. Makhathini, S. P. Noncolela, J. Ndayishimye, A. Netshiya, O. Shrinda, M. Wiedeking, and B. R. Zikhali, A fast-timing array of 2" x 2" LaBr3:Ce detectors for lifetime measurements of excited nuclear states, Nucl. Instrum. Meth. Phys. Res. A **1026**, 166195 (2022).

[23] M. Guttormsen, T. S. Tveter, L. Bergholt, F. Ingebretsen, and J. Rekstad, The unfolding of continuum γ-ray spectra, Nucl. Instrum. Meth. Phys. Res. A **374**, 371 (1996).

[24] S. Agostinelli, J. Allison, K. Amako, J. Apostolakis, H. Araujo, P. Arce, M. Asai, D. Axen, S. Banerjee, G. Barrand, F. Behner, L. Bellagamba, J. Boudreau, L. Broglia, A. Brunengo, H. Burkhardt, S. Chauvie, J. Chuma, R. Chytracek, G. Cooperman *et al.*, Geant4–a simulation toolkit, Nucl. Instrum. Meth. Phys. Res. A **506**, 250 (2003).

[25] V. W. Ingeberg, AFRODITE Geant4 model, 2022, https://github.com/vetlewi/AFRODITE.

[26] M. Guttormsen, T. Ramsøy, and J. Rekstad, The first generation of γ-rays from hot nuclei, Nucl. Instrum. Meth. Phys. Res. A **255**, 518 (1987).

[27] R. Capote, M. Herman, P. Obložinský, P. G. Young, S. Goriely, T. Belgya, A. V. Ignatyuk, A. J. Koning, S. Hilaire, V. A. Plujko, M. Avrigeanu, O. Bersillon, M. B. Chadwick, T. Fukahori, Z. Ge, Y. Han, S. Kailas, J. Kopecky, V. M. Maslov, G. Reffo *et al.*, RIPL - Reference Input Parameter Library for calculation of nuclear reactions and nuclear data evaluations, Nucl. Data Sheets **110**, 3107 (2009).

[28] T. Ericson, A statistical analysis of excited nuclear states, Nucl. Phys. **11**, 481 (1959).

[29] M. Guttormsen, S. Goriely, A. C. Larsen, A. Görgen, T. W. Hagen, T. Renstrøm, S. Siem, N. U. H. Syed, G. Tagliente, H. K. Toft, H. Utsunomiya, A. V. Voinov, and K. Wikan, Quasicontinuum γ decay of Zr 91,92: Benchmarking indirect (n,γ) cross section measurements for the s process, Phys. Rev. C **96**, 024313 (2017).

[30] J. E. Midtbø, A. C. Larsen, T. Renstrøm, F. L. Bello Garrote, and E. Lima, Consolidating the concept of low-energy magnetic dipole decay radiation, Phys. Rev. C **98**, 064321 (2018).

[31] T. von Egidy and D. Bucurescu, Systematics of nuclear level density parameters, Phys. Rev. C **72**, 044311 (2005).

[32] A. Gilbert and A. G. W. Cameron, A composite nuclear-level density formula with shell corrections, Can. J. Phys. **43**, 1446 (1965).

[33] T. von Egidy and D. Bucurescu, Experimental energy-dependent nuclear spin distributions, Phys. Rev. C **80**, 054310 (2009).

[34] C. Lederer, C. Massimi, E. Berthoumieux, N. Colonna, R. Dressler, C. Guerrero, F. Gunsing, F. Käppeler, N. Kivel, M. Pignatari, R. Reifarth, D. Schumann, A. Wallner, S. Altstadt, S. Andriamonje, J. Andrzejewski, L. Audouin, M. Barbagallo, V. Bécares, F. Bečvář *et al.*, 62Ni(n, γ) and 63Ni(n, γ) cross sections measured at the n_TOF facility at CERN, Phys. Rev. C **89**, 025810 (2014).

[35] S. F. Mughabghab, *Atlas of Neutron Resonances : Volume 1: Resonance Properties and Thermal Cross Sections Z = 1-60*, 6th ed., Atlas of Neutron Resonances (Elsevier Science, Amsterdam, 2018).

[36] J. Kopecky and M. Uhl, Test of gamma-ray strength functions in nuclear reaction model calculations, Phys. Rev. C **41**, 1941 (1990).

[37] J. Buchner, UltraNest - a robust, general purpose Bayesian inference engine, J. Open Source Software **6**, 3001 (2021).

[38] M. Guttormsen, K. O. Ay, M. Ozgur, E. Algin, A. C. Larsen, F. L. B. Garrote, H. C. Berg, L. C. Campo, T. Dahl-Jacobsen, F. W. Furmyr, D. Gjestvang, A. Görgen, T. W. Hagen, V. W.

Ingeberg, B. V. Kheswa, I. K. B. Kullmann, M. Klintefjord, M. Markova, J. E. Midtbø, V. Modamio *et al.*, Evolution of the γ-ray strength function in neodymium isotopes, Phys. Rev. C **106**, 034314 (2022).

[39] M. Markova, P. von Neumann-Cosel, A. C. Larsen, S. Bassauer, A. Gorgen, M. Guttormsen, F. L. BelloGarrote, H. C. Berg, M. M. Bjoroen, T. Dahl-Jacobsen, T. K. Eriksen, D. Gjestvang, J. Isaak, M. Mbabane, W. Paulsen, L. G. Pedersen, N. I. J. Pettersen, A. Richter, E. Sahin, P. Scholz, S. Siem, G. M. Tveten, V. M. Valsdottir, M. Wiedeking, and F. Zeiser, Comprehensive Test of the Brink-Axel Hypothesis in the Energy Region of the Pygmy Dipole Resonance, Phys. Rev. Lett. **127**, 182501 (2021).

[40] L. G. Moretto, A. C. Larsen, F. Giacoppo, M. Guttormsen, and S. Siem, Experimental first order pairing phase transition in atomic nuclei, J. Phys.: Conf. Ser. **580**, 012048 (2015).

[41] A. C. Larsen, N. Blasi, A. Bracco, F. Camera, T. K. Eriksen, A. Görgen, M. Guttormsen, T. W. Hagen, S. Leoni, B. Million, H. T. Nyhus, T. Renstrøm, S. J. Rose, I. E. Ruud, S. Siem, T. Tornyi, G. M. Tveten, A. V. Voinov, and M. Wiedeking, Evidence for the Dipole Nature of the Low-Energy γ Enhancement in Fe56, Phys. Rev. Lett. **111**, 242504 (2013).

[42] A. C. Larsen, M. Guttormsen, N. Blasi, A. Bracco, F. Camera, L. C. Campo, T. K. Eriksen, A. Görgen, T. W. Hagen, V. W. Ingeberg, B. V. Kheswa, S. Leoni, J. E. Midtbø, B. Million, H. T. Nyhus, T. Renstrøm, S. J. Rose, I. E. Ruud, S. Siem, T. G. Tornyi *et al.*, Low-energy enhancement and fluctuations of γ-ray strength functions in 56,57 Fe: Test of the Brink-Axel hypothesis, J. Phys. G: Nucl. Part. Phys. **44**, 064005 (2017).

[43] T. Renstrøm, H. T. Nyhus, H. Utsunomiya, R. Schwengner, S. Goriely, A. C. Larsen, D. M. Filipescu, I. Gheorghe, L. A. Bernstein, D. L. Bleuel, T. Glodariu, A. Görgen, M. Guttormsen, T. W. Hagen, B. V. Kheswa, Y. W. Lui, D. Negi, I. E. Ruud, T. Shima, S. Siem *et al.*, Low-energy enhancement in the γ-ray strength functions of Ge 73,74, Phys. Rev. C **93**, 064302 (2016).